Super-resolution imaging by resonant tunneling in anisotropic acoustic metamaterials

Aiping Liu and Xiaoming Zhou[a)]
Key Laboratory of Dynamics and Control of Flight Vehicle, Ministry of Education and School of Aerospace Engineering, Beijing Institute of Technology, Beijing 100081, China

Guoliang Huang
Department of Systems Engineering, University of Arkansas at Little Rock, Little Rock, Arkansas 72204

Gengkai Hu
Key Laboratory of Dynamics and Control of Flight Vehicle, Ministry of Education and School of Aerospace Engineering, Beijing Institute of Technology, Beijing 100081, China

(Received 23 November 2011; revised 21 March 2012; accepted 2 April 2012)

The resonant tunneling effects that could result in complete transmission of evanescent waves are examined in acoustic metamaterials of anisotropic effective mass. The tunneling conditions are first derived for the metamaterials composed of classical mass-in-mass structures. It is found that the tunneling transmission occurs when the total length of metamaterials is an integral number of half-wavelengths of the periodic Bloch wave. Due to the local resonance of building units of metamaterials, the Bloch waves are spatially modulated within the periodic structures, leading to the resonant tunneling occurring in the low-frequency region. The metamaterial slab lens with anisotropic effective mass is designed by which the physics of resonant tunneling and the features for evanescent field manipulations are examined. The designed lens interacts with evanescent waves in the way of the propagating wavenumber weakly dependent on the spatial frequency of evanescent waves. Full-wave simulations validate the imaging performance of the proposed lens with the spatial resolution beyond the diffraction limit. © *2012 Acoustical Society of America*.
[http://dx.doi.org/10.1121/1.4744932]

PACS number(s): 43.58.Ls, 43.40.Fz, 43.20.Ks [ANN] Pages: 2800–2806

I. INTRODUCTION

Conventional imaging systems capture propagating waves to produce images, while the sub-wavelength information of the objects cannot be collected at the image plane because the evanescent waves carrying object's fine features decay rapidly in the near field. The loss of evanescent wave components in the scattering fields is the fundamental reason of the diffraction limit of the conventional imaging system.[1] Many attempts have been made to explore lens systems with sub-wavelength images for several decades that will make significant impacts on the applications of the non-destructive testing and medical screening. In recent years, attention has been paid to the "superlens" designed with the metamaterial concept to overcome the diffraction limit.[2–4] Several mechanisms have been revealed by which metamaterial-based acoustic lenses could interact with evanescent waves in the way of enhancing or maintaining the evanescent field amplitudes. Ambati *et al.* proposed to enhance evanescent field amplitudes by exciting surface resonant states of the metamaterial lens with negative effective mass.[5] Evanescent waves can be efficiently coupled to the surface state, and their amplitudes are resonantly enhanced. Such superlens with negative effective mass can be designed in theory by use of acoustic metamaterials made of rubber-coated gold spheres in epoxy.[6] However, only parts of evanescent waves in the k space can be coupled to the surface modes, the field enhancements are non-uniform with respect to the spatial frequencies, so the ultimate image may be distorted.

Recently, metamaterial slab lenses with strongly anisotropic effective mass have been proposed to achieve uniform enhancements for all evanescent fields in the k space.[7] Effective mass of the lens has been made to approach infinity in the direction parallel to the slab interface so that the propagating wavenumber is weakly dependent on the parallel ones. Inside the lens, evanescent waves can be converted to the propagating ones and transferred to the outside of the lens. To achieve an extraordinary transmission of evanescent waves, the Fabry–Pérot resonant conditions should be satisfied,[7,8] which requires that the thickness of lens is equal to the integer number of half wavelength. To bring the lens size into a smaller scale than the operating wavelength, a different transmission mechanism has been proposed based on near-zero effective mass, and the superlens model made of such metamaterials has been designed to verify the imaging effect.[9] Based on such model, the super-resolution imaging due to the tunneling effect will be analyzed in this work. The underlying mechanism can be attributed to the strong spatial modulation of acoustic waves by locally resonant units of metamaterials.

Acoustic metamaterials are artificial composite materials with unusual macroscopic behaviors not readily observed in natural materials. Liu *et al.* first proposed the metamaterial with negative dynamic effective mass[10] that is composed of the

[a)]Author to whom correspondence should be addressed. Electronic mail: zhxming@bit.edu.cn

 0001-4966/2012/132(4)/2800/7/$30.00

rubber-coated lead spheres periodically distributed in an epoxy matrix. The resonant behavior of the building units can be well illustrated by a rigid mass attached inside to a mass-spring oscillator.[11] Negative effective mass can be defined around the resonant frequency of the building units to describe the antiphase effects between the applied force and acceleration response. It is important to note that the resonance of the building units could also produce extremely large positive effective mass just below the frequencies of negative effective mass. The large positive mass could result in the Bragg gap[12] due to strong spatial oscillations of wave fields within the periodic structures. Inspired by the peculiar macroscopic behaviors of acoustic metamaterials, the resonant tunneling effects for evanescent waves will be examined in this work. Here the tunneling effect means that evanescent waves, which normally decay in the near field, can penetrate the metamaterial barriers with complete transmission. For simplification, lattice metamaterials made of masses and springs will be analyzed first to demonstrate the resonant tunneling mechanisms. Then the acoustic super-resolution imaging at the different tunneling frequencies will be illustrated in the designed metamaterial lens.

II. RESONANT TUNNELING IN LATTICE METAMATERIALS

A. Anisotropic acoustic metamaterials

The subject of resonant tunneling is first studied in lattice metamaterials made of masses and springs. The geometry of the model is shown in Fig. 1, where metamaterials are modeled as periodic units composed of the classical mass-in-mass structures[11] attached with two springs of equal spring constant $2K$. Lattice metamaterials are sandwiched between the same fluid mediums with the mass density ρ_0 and the sound velocity c_0. To illustrate the transmission of evanescent waves, plane acoustic waves are obliquely incident on the metamaterials with parallel wavenumber k_y. The mass-in-mass structures are all fixed in the y direction. The anisotropic effective mass matrix is written as

$$\tilde{m}_{\text{eff}} = \begin{bmatrix} m_{\text{eff}} & 0 \\ 0 & \infty \end{bmatrix},$$

where $m_{\text{eff}} = m_0 + (m_1/(1-\omega^2/\omega_0^2))$, with $\omega_0 = \sqrt{G/m_1}$. The resonant tunneling effects will be examined in the frequency range below ω_0.

B. Transfer matrix of the acoustic metamaterials

Transfer functions describe the transmission properties of propagating and evanescent waves in the lattice metamaterials. To calculate the transfer functions, it is useful to define the transfer matrix $\boldsymbol{M}$ of metamaterials to be the matrix relation between displacements u and forces F evaluated on the input surface and those on the output surface, as depicted in Fig. 2. The transfer matrix of one unit cell is defined to be

$$\begin{bmatrix} u^r \\ F^r \end{bmatrix} = \boldsymbol{M} \begin{bmatrix} u^l \\ F^l \end{bmatrix}, \tag{1}$$

where the superscripts r, l represent, respectively, the right and left boundaries of the unit cell, and

$$\boldsymbol{M}_1 = \begin{bmatrix} \dfrac{2K - m_{\text{eff}}\omega^2}{2K} & \dfrac{4K - m_{\text{eff}}\omega^2}{4K^2} \\ -m_{\text{eff}}\omega^2 & \dfrac{2K - m_{\text{eff}}\omega^2}{2K} \end{bmatrix}. \tag{2}$$

Then the transfer matrix of N units is written as

$$\boldsymbol{M}_N = (\boldsymbol{M}_1)^N. \tag{3}$$

The dispersion relation can be obtained by imposing the periodic condition on the unit cell

$$\begin{bmatrix} u^r \\ F^r \end{bmatrix} = e^{iqL} \begin{bmatrix} u^l \\ F^l \end{bmatrix}, \tag{4}$$

where q is the Bloch wavenumber and L is the length of one unit. The dispersion relation can be obtained by combining Eqs. (2) and (4) as

$$\det\left[\boldsymbol{M}_1 - \boldsymbol{I}e^{iqL}\right] = 0, \tag{5}$$

where $\boldsymbol{I}$ is the second-order identity tensor. Equation (5) results in

$$m_{\text{eff}}\omega^2 = 4K\,sin^2(qL/2). \tag{6}$$

The x-component displacement fields u of the ambient fluids in the incident and transmitting regions are expressed, respectively, as

$$u(x,y) = (e^{ik_{0x}x} + \text{Re}^{-ik_{0x}x})e^{ik_y y},\ x \le 0, \tag{7a}$$

$$u(x,y) = \text{Te}^{ik_{0x}(x-NL)}e^{ik_y y},\ x \ge NL, \tag{7b}$$

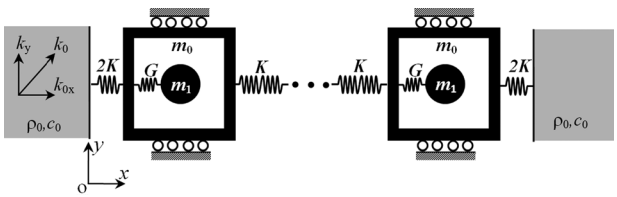

FIG. 1. The model for analyzing the resonant tunneling in lattice metamaterials.

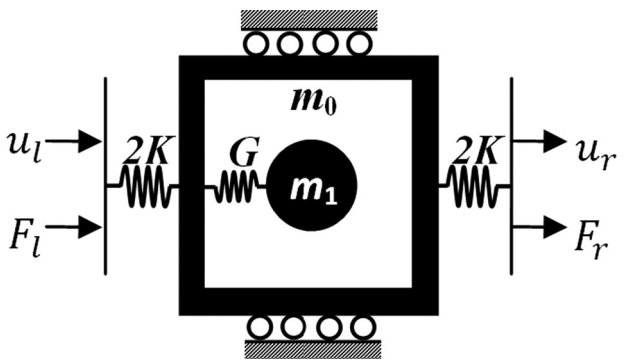

FIG. 2. Definition of the transfer matrix in one unit cell.

where $k_{0x} = \sqrt{k_0^2 - k_y^2}$, R and T are complex amplitudes of the reflected and transmitted waves.

Consider the continuous conditions of displacements and forces in the direction normal to the metamaterial surface, the equation can be written as

$$\begin{bmatrix} T \\ iQT \end{bmatrix} = \boldsymbol{M}_N \begin{bmatrix} 1+R \\ iQ(1-R) \end{bmatrix}, \tag{8}$$

where $Q = \rho_0 c_0^2 k_{0x} A$, and A is the area of the interface $x = 0$. From Eq. (8), the transfer function T can be written as

$$T(k_y) = \frac{2Q}{Q(M_N^{11} + M_N^{22}) - i(Q^2 M_N^{12} - M_N^{21})}, \tag{9}$$

where it is defined that

$$\boldsymbol{M}_N = \begin{bmatrix} M_N^{11} & M_N^{12} \\ M_N^{21} & M_N^{22} \end{bmatrix}. \tag{10}$$

C. Resonant tunneling conditions

Resonant tunneling conditions correspond to complete transmission of evanescent waves with $k_y > k_0$. Equation (9) could be simplified to get the analytic expression of tunneling conditions. It is found that $\boldsymbol{M}_1$ is a unimodular matrix satisfying $\det[\boldsymbol{M}_1] = 1$, the Nth power of a unimodular matrix follows the matrix identity

$$[\boldsymbol{M}_1]^N = \begin{bmatrix} M_1^{11} U_{N-1} - U_{N-2} & M_1^{12} U_{N-1} \\ M_1^{21} U_{N-1} & M_1^{22} U_{N-1} - U_{N-2} \end{bmatrix}, \tag{11}$$

where $U_N = \sin[(N+1)qL]/\sin(qL)$. Substituting Eq. (11) into Eq. (9), the transfer function is rewritten as

$$T(k_y) = \frac{2Q}{2Q\cos(NqL) - i(Q^2 M_1^{12} - M_1^{21})\sin(NqL)/\sin(qL)}. \tag{12}$$

According to Eq. (12), the tunneling conditions are found to be

$$NqL = m\pi, \ m = 1, 2, \ldots, N-1. \tag{13}$$

It is found that the condition (13) also results in complete transmission of propagating waves with $k_y > k_0$. So Eq. (13) means the complete transmission of both propagating and evanescent waves. The derived tunneling conditions are only satisfied when metamaterials have over two unit cells. There are $N-1$ tunneling conditions for metamaterials comprising N units. Define the wavelength of a lattice wave in the metamaterials to be $\lambda = 2\pi/q$. The tunneling conditions (13) can also be expressed as

$$NL = m\frac{\lambda}{2}, \ m = 1, 2, \ldots, N-1. \tag{14}$$

D. Bandwidth of the tunneling transmission

From Eq. (14), complete transmission occurs if the total length of metamaterials is an integral number of half-wavelengths. When the resonant tunneling does not occur at exactly integral multiples of half-wavelengths, transmission amplitudes will be reduced because of the phase shift of reflections from each individual unit, resulting in the finite bandwidth of the imaging system designed with this mechanism.

The bandwidth of tunneling transmission can be evaluated by determination of the finite width of transmission peaks at their half-maximum values. Consider the case of two units ($N = 2$) involved in the metamaterials. From Eq. (12), the transmission is given by

$$T = \frac{1}{\cos(2qL) - i[(Q/2K)(1+\cos qL) + (2K/Q)(1-\cos qL)]\cos(qL)}. \tag{15}$$

In the normal incident case $k_y = 0$, let $|T|^2 = 0.5$, we get

$$\cos(qL) = \frac{Q^2 - 4K^2}{Q^2 + 4K^2}. \tag{16}$$

From Eqs. (6) and (16), the bandwidth $\delta\omega$ between half-maximum values of the transmission peak is approximately

$$\delta\omega \approx \sqrt{\frac{2K}{m_{\text{eff}}}}\left(1 - \sqrt{1 - \left|\frac{Q^2 - 4K^2}{Q^2 + 4K^2}\right|}\right), \tag{17}$$

where the frequency dependent parameters m_{eff} and Q are assumed to take their values at the tunneling frequency. It is seen in Eq. (17) that the bandwidth is inversely proportional to effective mass. Because effective mass of metamaterials is dependent on frequency, the bandwidth may be different at different tunneling frequencies.

E. Numerical results and discussions

As an example, consider the following parameters $G/K = m_1/m_0 = 1$, $c_0 = \sqrt{K/(A\rho_0)} = \sqrt{10}$ m/s. Figure 3(a) shows the effective mass m_{eff} (dashed line) and dispersion curve qL (solid line) as the function of frequency. It is seen that the waves cannot exist in the frequencies of negative effective mass due to the decaying nature of wave field amplitudes. Note that the local resonance induces not only a negative effective mass but also an extremely large mass just

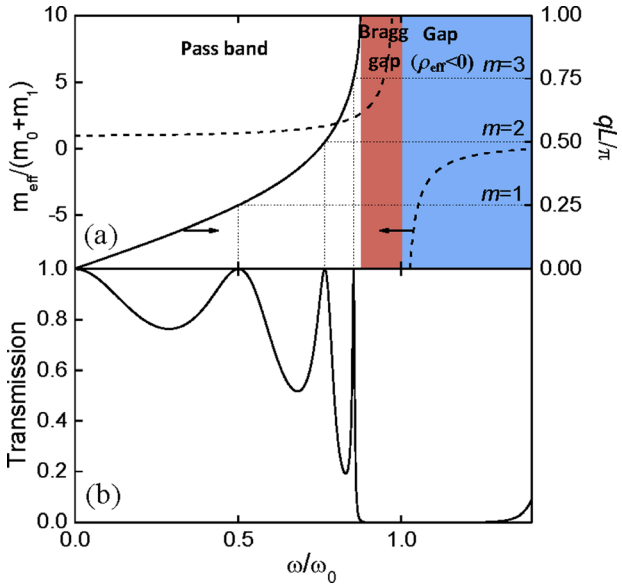

FIG. 3. (Color online) (a) Effective mass m_{eff} and Bloch wavenumber qL versus frequencies; (b) the transmission coefficients of the metamaterials with four units.

below ω_0. The large mass results in strong spatial oscillation of wave fields within the periodic structures, giving rise to the Bragg gap $qL = \pi$. This low-frequency Bragg gap might be different from the common one because the Bragg resonance is occurring in the sub-wavelength scale, and it is designed based on the local resonances in the metamaterial concept.[12] In the pass band below the Bragg gap, the resonant tunneling conditions could be satisfied. Figure 3(b) gives the transmission coefficients of waves normally incident on the lattice metamaterials composed of four units ($N = 4$). Three transmission peaks are observed at frequencies where the tunneling conditions $qL = \pi/4, \pi/2, 3\pi/4$ are satisfied.

The contour plot of transmission amplitude distributions of plane waves in different parallel wavenumber k_y and frequencies ω/ω_0 is shown in Fig. 4. At three tunneling frequencies, complete transmission occurs for both propagating

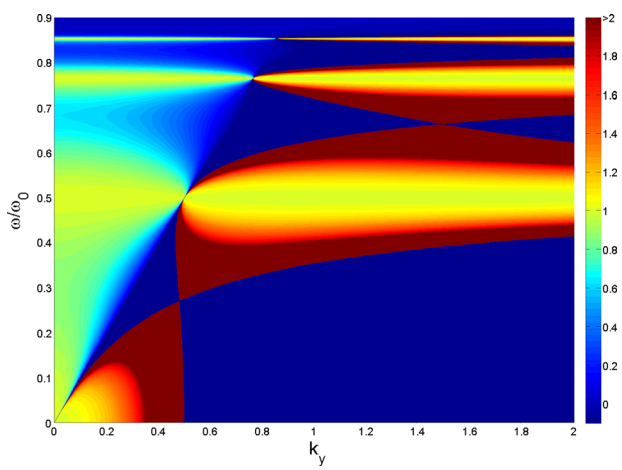

FIG. 4. (Color online) The contour plot of transmission amplitude distributions for plane waves of different parallel wavenumber k_y and frequencies ω/ω_0 incident on the lattice metamaterial with four periodic units.

and evanescent waves in the k space. This behavior can be utilized to realize acoustic super-resolution imaging at the tunneling frequencies. In addition, the bandwidth of tunneling transmission becomes narrower at higher frequencies because of increasing effective mass of the building units as predicted by Eq. (17). This has implications to widening the operating bandwidth of the imaging system designed by metamaterials with dispersive effective mass.

In this section, the tunneling conditions of the complete transmission for both propagating and evanescent waves are derived in lattice metamaterials composed of mass-spring structures with anisotropic effective mass. Because evanescent field amplitudes are prevented from decaying at tunneling frequencies, the resonant tunneling has important applications to acoustic imaging with the spatial resolution beyond the diffraction limit. Based on preceding analyses, a continuum metamaterial superlens will be designed, and the super-resolution imaging will be verified in the next section.

III. REALIZATION OF SUPER-RESOLUTION IMAGING

A. The model of the superlens

The model of the superlens is shown in Fig. 5. The lens consists of rigid and fixed slabs placed with a periodic array of slits partially filled by elastic layers. The width of slit is a, and the lattice constant of the grating period is d. In each slit, elastic layers of the thickness w are separated by cavities, forming a periodic array with lattice parameter s. The total thickness of the lens is $h = Ns$. Consider the case where the periodicities d and s are much less than the operating wavelength, the proposed lens is well characterized by acoustic metamaterial with anisotropic effective mass. This configuration has been examined for super-resolution imaging based on the mechanism of nearly zero effective mass; here the tunneling mechanism will be analyzed.

B. Normal transmission properties

Consider the following parameters for the lens: $a = 4\,\text{mm}$, $d = 5\,\text{mm}$, $w = 2\,\text{mm}$, and $s = 10\,\text{mm}$, and the elastic layer is the rubber with Young's modulus 0.1 MPa, Poission's ratio 0.49, and mass density $1100\,\text{kg/m}^3$. Mass density and sound velocity of the air surrounding and cavities are taken to be $\rho_0 = 1.25\,\text{kg/m}^3$ and $c_0 = 343\,\text{m/s}$. The fixed and rigid slabs ensure that effective mass of the lens is infinite in the y direction. In the x direction, the effective mass evaluated in the unit cell can be retrieved by field averaging methods[13] and is shown in Fig. 6(a) as the dashed line. It is found that negative effective mass occurs below the

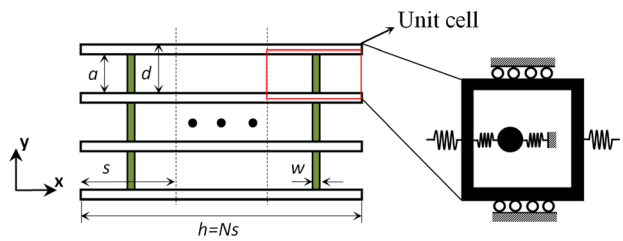

FIG. 5. (Color online) The model of the designed superlens.

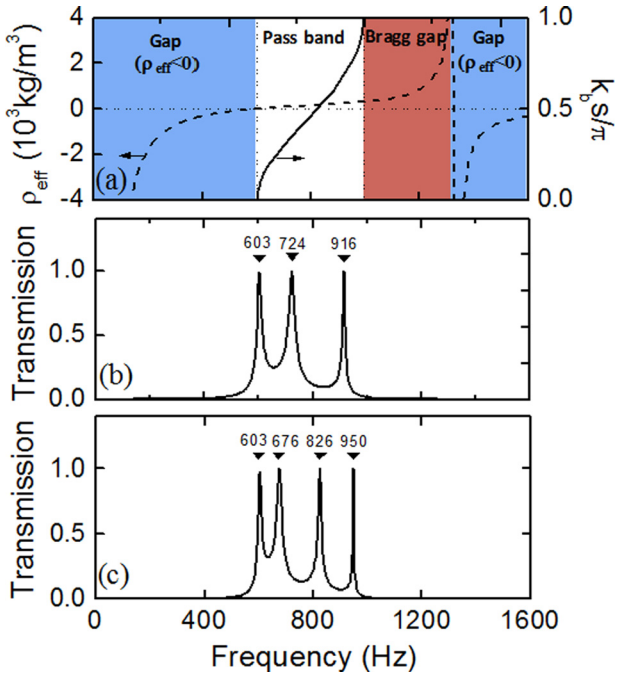

FIG. 6. (Color online) (a) Effective mass ρ_{eff} and Bloch wavenumber k_b versus frequencies evaluated in the unit cell of the proposed lens and the transmission coefficients of the lens with (b) three and (c) four units.

first-order eigenfrequency of the clamped plate. The physics has been attributed to the clamped boundary condition, which imposes the spring-like constraints by the shear resistance of the plate.[14] The second-order resonance of the clamped plate can be characterized by the classical mass-in-mass structures. So the variation of effective mass of the clamped plate as function of frequency can be understood from the equivalent mass-spring structure as shown in the right panel of Fig. 5, where the inner mass in the mass-in-mass structure is constrained by a spring. Figure 6(a) shows

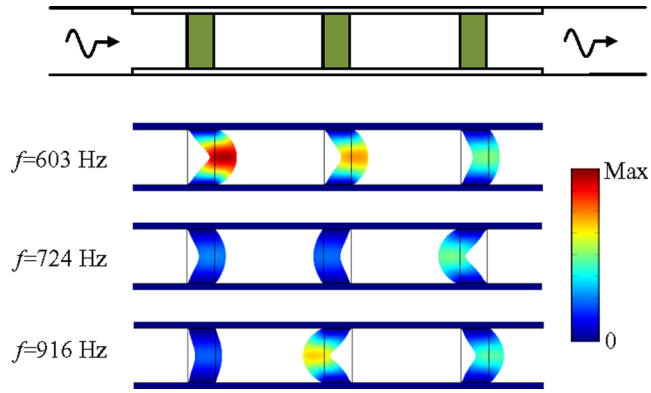

FIG. 7. (Color online) Snapshot of the deformed shapes of the plates at three frequencies, 603, 724, and 916 Hz, for acoustic waves normally incident on the metamaterial lens with three units ($N = 3$).

the lowest branch of the dispersion curves (solid line) computed in the unit cell by use of periodic conditions imposed on the left and right boundaries. It is seen that the waves cannot exist in the frequencies of negative effective mass and in the Bragg gap. The resonant tunneling effects can be examined in the pass band as addressed in the preceding section.

Figure 6(b) shows the normal transmission coefficients of the metamaterial lens with three units ($N = 3$). It can be found that the transmission is greatly lowered in the gap region. In the pass band, three distinct transmission peaks are observed at 603, 724, and 916 Hz. The first peak is the extraordinary transmission due to near-zero effective mass, and the latter two are induced, respectively, by the resonant tunneling of the odd and even modes. To capture the underlying physics of three transmission peaks, the contour plots of the deformations of the plates are plotted in Fig. 7 at those three frequencies. Three transmission peaks can be differentiated from bulk deformations of the cavity. For the first peak (603 Hz), the clamped plates oscillate in the same

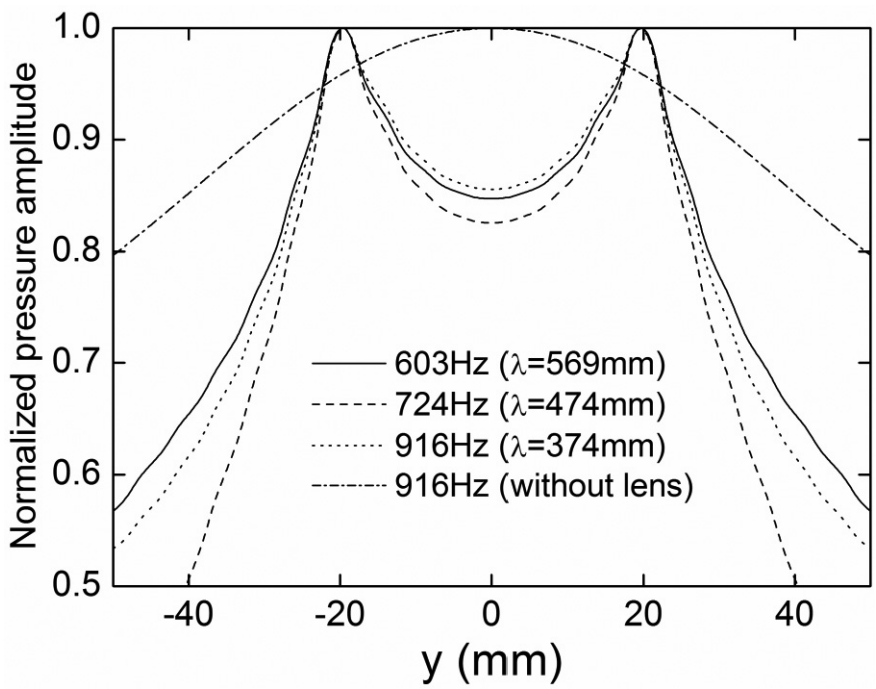

FIG. 8. Normalized pressure amplitudes in the image plane of the designed lens in front of which two monopole line sources are placed by the separation 40 mm and operating at 603, 724, and 916 Hz as well as the pressure distributions at 916 Hz without the lens.

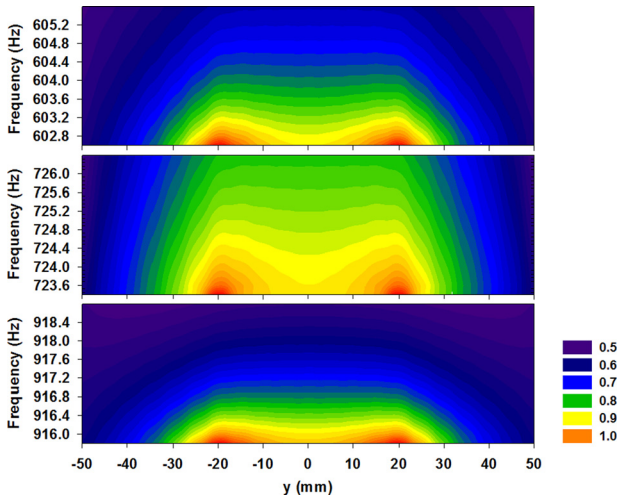

FIG. 9. (Color online) Contour plots of pressure amplitude distributions in the image plane at frequencies around 603, 724, and 916 Hz.

phase, then the phase shift across all units is zero. The zero phase shift has been explained by zero effective mass[15] and results in the air cavity being less deformed. At the second peak (724 Hz), the left cavity becomes compressed due to the left two plates vibrating in the opposite phase. Because the right cavity remains undeformed, the vibrations of the first and third plates are in the opposite phase. Thus the transmission in the odd mode is $T=-1$, as also predicted by Eq. (12). For the third peak (916 Hz), adjacent plates move in the opposite phase as a result of the remarkable bulk deformation of both cavities. Because the cavity length is far less than the operating wavelength, the air cavity behaves like the spring to connect the unit cell, and the possible mass-spring equivalence can also be imagined to discover above mechanisms. The normal transmission coefficients of the metamaterial lens with four units ($N=4$) are shown in Fig. 6(c). By comparison with Fig. 6(b), the peak transmission frequency at near-zero effective mass is unchanged because of unified movements of each plate. The frequencies of tunneling transmission will be changed due to different combinations of modes of cavity deformation.

The designed lens can be modeled as an acoustic metamaterial with anisotropic effective mass[9] and characterized by the general dispersion relation $k_x^2/\rho_x + k_y^2/\rho_y = \omega^2/B$, where B is the modulus. Fixed slabs ensure that $\rho_y \to \infty$, and the propagating wavenumber k_x is weakly dependent on the parallel wavenumber k_y. Thus the complete transmission designed in the normal incident case will be operative for other incident waves with k_y covering the evanescent wave space. The super-resolution imaging of the lens will be verified in the following.

C. Imaging performance of the superlens

To verify the imaging effect, two monopole line sources separated by 40 mm are placed in front of the designed lens at the distance 1 mm, and the image plane is taken 1 mm behind the lens. The normalized pressure amplitudes in the image plane of the designed lens are shown in Fig. 8 for three operating frequencies, 603, 724, and 916 Hz. By comparison to the pressure distributions without the lens, two sources can be clearly resolved in the presence of the designed lens at near-zero effective mass and tunneling frequencies, confirming the super-resolution imaging beyond the diffraction limit. Figure 9 shows the contour plots of pressure amplitude distributions in the image plane at frequencies around 603, 724, and 916 Hz to evaluate the imaging bandwidth. Because the tunneling transmission is based on the resonant effect, the operating bandwidth is quite narrow. Note that the wider bandwidth at lower tunneling frequencies is due to smaller effective mass as implied by Eq. (17). This suggests that the operating bandwidth of imaging may be widened by making effective mass of the building units as small as possible.

IV. CONCLUSIONS

The current effort is an extension of work reported earlier by Zhou *et al.*[9] In that work, the efficient transmission of evanescent waves based on near-zero effective mass is studied. The model of metamaterial lens is proposed to verify the super-resolution imaging at low frequencies. Here based on the same model, the tunneling effects that could lead to complete transmission of evanescent waves are analyzed. To discover the underlying mechanism, an analytic model is developed for the lattice metamaterials made of mass-in-mass structures. The tunneling conditions are derived to be $NqL = m\pi$, which is similar to the Fabry–Pérot resonant conditions for the homogeneous materials.[7,8] It is interesting to note that the peak transmission frequencies in Figs. 6(b) and 6(c) approximately satisfy $Nk_bs = m\pi$, showing the correlation between the designed lens and the lattice metamaterials. Evaluation on the bandwidth is also proposed to explain the decreasing of the bandwidth of imaging induced by the increasing of effective mass. In general, the designed slab lens captures evanescent waves because of infinite effective mass in the direction parallel to the slab interface. The efficient transmission of evanescent fields could be realized based on either near-zero mass or tunneling resonances. The lens capable of these features is able to produce images with the spatial resolution beyond the diffraction limit.

ACKNOWLEDGMENT

This paper was supported by the National Natural Science Foundation of China (Grant Nos. 10832002, 11172038, and 11072031) and the Natural Science Foundation EAGER program (Grant No. 1037569).

[1]M. Born and E. Wolf, *Principles of Optics*, 7th ed. (Cambridge University Press, Cambridge, UK, 1999), Chap. 8, pp. 412–516.
[2]J. B. Pendry, "Negative refraction makes a perfect lens," Phys. Rev. Lett. **85**, 3966–3969 (2000).
[3]S. Guenneau, A. Movchan, G. Pétursson, and S. A. Ramarkrishna, "Acoustic metamaterials for sound focusing and confinement," New J. Phys. **9**, 399 (2007).
[4]S. Zhang, L. Yin, and N. Fang, "Focusing ultrasound with an acoustic metamaterial network," Phys. Rev. Lett. **102**, 194301 (2009).
[5]M. Ambati, N. Fang, C. Sun, and X. Zhang, "Surface resonant states and superlensing in acoustic metamaterials," Phys. Rev. B **75**, 195447 (2007).

[6]K. Deng, Y. Ding, Z. He, H. Zhao, J. Shi, and Z. Liu, "Theoretical study of subwavelength imaging by acoustic metamaterial slabs," J. Appl. Phys. **105**, 124909 (2009).
[7]J. Zhu, J. Christensen, J. Jung, L. Martin-Moreno, X. Yin, L. Fok, X. Zhang, and F. J. Garcia-Vidal, "A holey-structured metamaterial for acoustic deep-subwavelength imaging," Nat. Phys. **7**, 52 (2010).
[8]F. Liu, F. Cai, S. Peng, R. Hao, M. Ke, and Z. Liu, "Parallel acoustic near-field microscope: A steel slab with a periodic array of slits," Phys. Rev. E **80**, 026603 (2009).
[9]X. Zhou and G. Hu, "Superlensing effect of an anisotropic metamaterial slab with near-zero dynamic mass," Appl. Phys. Lett. **98**, 263510 (2011).
[10]Z. Liu, X. Zhang, Y. Mao, Y. Y. Zhu, Z. Yang, C. T. Chan, and P. Sheng, "Locally resonant sonic materials," Science **289**, 1734 (2000).
[11]G. W. Milton and J. R. Willis, "On modifications of newton's second law and linear continuum elastodynamics," Proc. R. Soc. London, Ser. A **463**, 855–880 (2007).
[12]Y. Xiao, B. R. Mace, J. Wen, and X. Wen, "Formation and coupling of band gaps in a locally resonant elastic system comprising a string with attached resonators," Phys. Lett. A **375**, 1485–1491 (2011).
[13]X. Zhou and G. Hu, "Analytic model of elastic metamaterials with local resonances," Phys. Rev. B **79**, 195109 (2009).
[14]S. Yao, X. Zhou, and G. Hu, "Investigation of the negative-mass behaviors occurring below a cut-off frequency," New J. Phys. **12**, 103025 (2010).
[15]S. Yao, X. Zhou, and G. Hu, "Experimental study on negative effective mass in a 1D mass–spring system," New J. Phys. **10**, 043020 (2008).